Precision Determination of Isotope Shifts in Ytterbium and Implications for New Physics

N. L. Figueroa
Johannes Gutenberg-Universität Mainz, Helmholtz-Institut Mainz, GSI Helmholtzzentrum für Schwerionenforschung, 55128 Mainz, Germany

J. C. Berengut, V. A. Dzuba, and V. V. Flambaum
School of Physics, University of New South Wales, Sydney, New South Wales 2052, Australia

D. Budker and D. Antypas*
Johannes Gutenberg-Universität Mainz, Helmholtz-Institut Mainz, GSI Helmholtzzentrum für Schwerionenforschung, 55128 Mainz, Germany

(Received 2 November 2021; accepted 25 January 2022; published 17 February 2022)

We report measurements of isotope shifts for the five spinless Yb isotopes on the $6s^2\ {}^1S_0 \rightarrow 5d6s\ {}^1D_2$ transition using Doppler-free two-photon spectroscopy. We combine these data with existing measurements on two transitions in Yb^+ [Counts *et al*. Phys. Rev. Lett. **125**, 123002 (2020)], where deviation from King-plot linearity showed hints of a new bosonic force carrier at the 3σ level. The combined data strongly reduce the significance of the new-physics signal. We show that the observed nonlinearity in the joint Yb/Yb^+ King-plot analysis can be accounted for by the deformation of the Yb nuclei.

DOI: 10.1103/PhysRevLett.128.073001

Introduction—Precision measurements in atomic systems offer ways to study particle physics at low energy [1–3] and complement work involving high-energy accelerators, neutrino studies, and astrophysical observations. Indeed, a number of experiments employing atomic or molecular probes have yielded a range of tests of fundamental principles and searches for physics beyond the standard model (SM) (see review in Ref. [4] and references therein). The role of precision spectroscopy in such work is further emphasized by recent ideas pointing to the manifestation of several beyond-SM physics scenarios in the isotope shifts (IS) of atomic spectra [5,6].

The IS in the frequency of an atomic transition are approximately linearly correlated with IS observed in another transition. This linearity in the so-called King-plot analysis [7,8] is used, for example, to extract the variation of nuclear charge radii from atomic spectra [9]. While deviations from linearity have long been known [10] in cases where subdominant nuclear effects cannot be neglected, the concept of nonlinearity (NL) has been recently revisited. As pointed out in [6], NL may arise due to beyond-SM interactions, such as the exchange of light force mediators between the electron and neutron [11]. Such interaction is invariant under spatial inversion (it is parity even) and can be sensitively probed for a mediator with Compton wavelength greater than the size of the nucleus, i.e., a mass $\lesssim 100\ \mathrm{MeV}/c^2$ [6,11]. Its parity-odd counterpart has been explored with atomic parity violation studies [12–14].

Following the ideas in Refs. [5,11], in Ref. [6] a framework was established for constraining new electron-neutron interactions using bounds on King-plot NL. The predictive power of the method, however, depends on the size of SM nuclear effects, that may also give rise to NL. Such effects were studied in Ref. [15], while in Ref. [16], it was shown that the limitations due to SM effects introducing NL can be mitigated if IS data from more than two transitions are combined in a generalized King-plot analysis.

As the availability of high-accuracy IS data enables probing for new bosons, several efforts were initiated to this end [17–23], dramatically improving the measurement accuracy previously limited to ≈100 kHz in the IS [24]. Most notably, two experiments with Yb^+ [21] and Ca^+ [22] reported on high-precision IS measurements, each employing five stable nuclear-spin-zero isotopes [25]. With these two experiments demonstrating comparable sensitivity to new physics (NP), it is intriguing that no King-plot NL was found in the Ca^+ work, but NL at the 3σ level was observed in Yb^+. This discrepancy hints at nuclear effects as the source of the NL in Yb^+, with the quadratic field shift suggested as a possible cause in Ref. [21] and the influence of nuclear deformation on the field shift proposed in Ref. [26].

While modeling nuclear effects is needed to gain insight into the cause of the observed Yb^+ NL, further precision IS data may allow separation of the SM and NP effects in a model-independent way [16]. Here we report on IS spectroscopy carried out in the $6s^2\ {}^1S_0 \rightarrow 5d6s\ {}^1D_2$ transition of neutral Yb, employing all five spinless isotopes. The data are combined with those of Ref. [21] to provide a joint Yb/Yb^+ King-plot analysis [16]. Since the two systems have the same

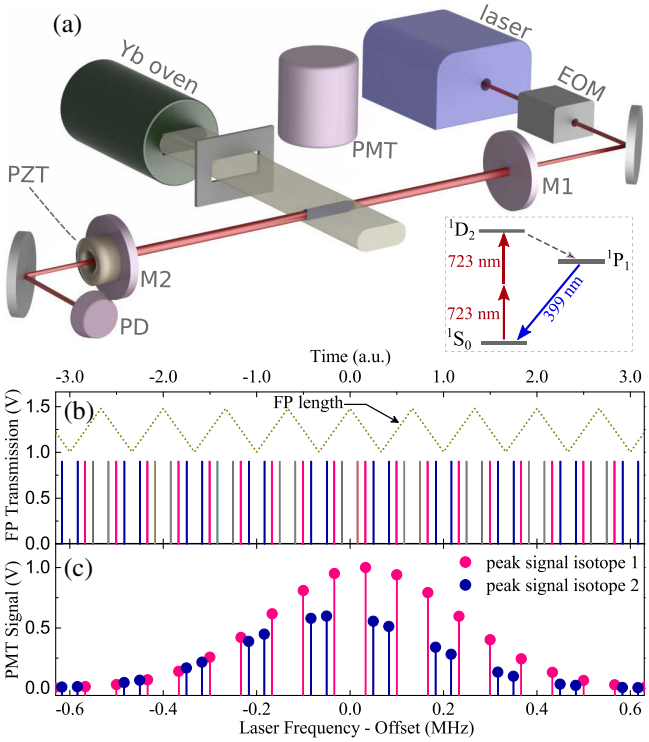

FIG. 1. Apparatus and spectrum measurement method. (a) Atomic beam setup for intracavity $^1S_0 \rightarrow {}^1D_2$ spectroscopy. EOM: electro-optic modulator; M1, M2: FP cavity mirrors; PMT: photomultiplier; PZT: piezoelectric transducer; PD: photodiode. (b) Simulated FP transmission signal, corresponding to the FP length being rapidly modulated (dotted triangle wave). The carrier (pink) and a first-order sideband (blue) are used to excite a pair of Yb isotopes, while the other first-order sideband (gray) is not resonant with atoms. (c) Simulated fluorescence of the atomic beam, resulting from the FP resonances shown in (b).

nucleus but different electronic structure, this IS comparison offers a way to evaluate modeling of higher-order nuclear effects, since the IS is generally different for the energy levels of the neutral and ionic Yb.

Experiment—Two-photon, Doppler-free spectroscopy [27] is carried out to extract the IS among the five spinless Yb isotopes (with mass number A-abundance: 176%–12.9%, 174%–31.9%, 172%–21.8%, 170%–3%, 168%–0.1%). The $6s^2\ {}^1S_0 \rightarrow 5d6s\ {}^1D_2$ transition, of ≈24 kHz natural linewidth [28], is excited in an atomic beam [Fig. 1(a)] with light at $\lambda \approx 723$ nm and detected via fluorescence at 399 nm, emitted in the second step of the $5d6s\ {}^1D_2 \rightarrow 6s6p\ {}^1P_1 \rightarrow 6s^2\ {}^1S_0$ cascade [Fig. 1(a)]. Only the component between the $m = 0 \rightarrow m' = 0$ magnetic sublevels is driven, using linear polarization for the optical field set along a $B \approx 4$ G applied magnetic field.

Our spectroscopy scheme employs two key features, implemented to minimize systematic effects from imperfections in the laser frequency calibration, and due to the first-order Doppler effect. First, a pair of isotopes to be measured for their IS is excited concurrently [20], using phase-modulated light which is produced with an electro-optic modulator that imposes frequency sidebands at the nominal IS frequency. The resulting optical field has spectral components $\nu_L = \nu_C \pm n\nu_m$, where ν_C is the carrier, $n = 0, 1, 2, \ldots$ is the sideband order, and ν_m is the frequency of the phase modulation, nominally set to match the IS frequency. To excite a pair of isotopes, the carrier and one of the sidebands with $n = 1$ are typically used.

The second key feature is that atoms are excited within a scanning Fabry-Pérot (FP) cavity. Since the counter-propagating components of the intracavity 723-nm field have well-matched wave fronts, the first-order Doppler shift is suppressed. The FP has another essential role. It allows one to temporally separate excitation of the isotopes being probed and detect the respective fluorescence signals in discrete channels; this enables "simultaneous" probing of both isotopes. Figures 1(b) and 1(c) illustrate this. As the FP length is rapidly scanned while the laser frequency is slowly swept across the S-D resonance, the various spectral components of light become resonant in the FP at different times; thus the two isotopes are probed in a rapid, but resolved time sequence. We monitor the FP transmission to gate detection using the respective FP fringes as gates. The peak signal within a gate is used to construct a line shape profile for each isotope.

To extract the IS, the frequency ν_m^0 is determined which yields a null frequency offset between the two isotope line shapes (see the Supplemental Material [29]). In the absence of systematics, the IS for the two-photon transition is $\delta\nu = 2\nu_m^0$. During a measurement run, line shapes for a given isotope pair are recorded for many values of ν_m in a range $\nu_m^0 \pm 10$ kHz. Fitting to the line shapes is done to determine their frequency offset and its variation with ν_m, in order to extract ν_m^0. The $\pm 2 \times 10$ kHz variation of the relative line shape offset is a small fraction of the observed ≈800 kHz transition width, which is limited by the transit time of atoms through the intracavity field [30]. With the line shapes practically overlapping during the laser sweep, systematics due to nonlinearity of the sweep are avoided (see the Supplemental Material [29]).

Several unwanted effects may introduce systematic shifts and require careful treatment (see the Supplemental Material [29]). Some are related to the ac-Stark effect. For the typical intracavity power of 5 W, it causes a shift of order of 20 kHz to the line shapes. With active stabilization of the carrier-sideband power ratio, the ratio is kept to unity to within 0.1%, and the residual mismatch is recorded and included in the analysis. However, parasitic interferences, such as for example between the fundamental transverse cavity mode and high-order modes, can, in principle, result in different intracavity intensity experienced by the two isotopes [31]. To eliminate potential shifts, data are taken at many powers, and extrapolation to zero power is done to extract the IS.

Another complication arises due to the multiple frequency components in the light injected into the FP. While a single component is resonant in the FP at a given time, one of the off-resonant components entering the FP due to the finite reflectivity of the input mirror (≈96.5%) acts with the resonant component to cause small, but measurable excitation of the "unwanted" isotope within the detection channel of the isotope primarily being measured. For example, when the first-order sideband of frequency $\nu_L = \nu_C + \nu_m$ is resonant and excites an isotope at frequency $2(\nu_C + \nu_m)$, due to the off-resonant sideband with $\nu_L' = \nu_C - \nu_m$, Doppler-free excitation at frequency $\nu_L + \nu_L' = 2\nu_C$ also occurs. This unwanted background signal has a small impact on extracting the IS between isotopes of similar abundance (e.g., ^{174}Yb/^{172}Yb), but substantial impact if the abundance varies drastically (e.g., ^{170}Yb/^{168}Yb). In the former case, we correct the IS measurements using Monte Carlo simulations of the effect; in the latter, we measure the backgrounds and correct the data accordingly.

To check for unaccounted for effects and ensure consistency of measurements, data are taken under a variety of conditions, for example, with FPs of different lengths, alternating use of the first-order sidebands, and at different Yb oven temperatures. The obtained accuracy in the IS, measured for the four pairs of adjacent mass, is ≈300 Hz (710 Hz for the low-abundance pair ^{170}Yb/^{168}Yb), and is limited by statistical uncertainty. Additional checks using the two first-order sidebands to probe the pairs ^{176}Yb − ^{172}Yb and ^{172}Yb − ^{168}Yb are consistent with the main dataset to within 0.3σ and 1.4σ, respectively. Our main experimental results are summarized in Table I.

King plots.—To a good approximation, the IS of a transition i is given by

$$\delta\nu_i^{AA'} = F_i \delta\langle r^2\rangle^{AA'} + K_i \mu^{AA'}, \quad (1)$$

TABLE I. Isotope shifts of the $^1S_0 \to {}^1D_2$ transition of Yb. The main results are listed in the first four rows and are used in King-plot analysis, while the remaining are complementary measurements used to check experimental consistency. The shift is defined as $\delta\nu^{AA'} = \nu^A - \nu^{A'}$.

Isotope pair (A-A')	Measured $\delta\nu^{AA'}$ (kHz)	Method[a]
168–170	1781785.36(71)	C-S[b]
170–172	1672021.51(30)	C-S
172–174	1294454.44(24)	C-S
174–176	1233942.19(31)	C-S
168–172	3453805.27(83)	S-S
172–176	2528396.50(34)	S-S

[a]C-S: measurement with use of carrier and first-order sideband fields; S-S: with use of the first-order sidebands.
[b]Isotope with $A = 168$ was always excited by the carrier, in order to mitigate the effects of parasitic backgrounds in the measurements (see the Supplemental Material [29]).

where $\delta\langle r^2\rangle^{AA'}$ is the change in nuclear mean-square charge radius between isotopes A and A', $\mu^{AA'} = 1/m_A - 1/m_A'$ is the change in inverse nuclear mass, and F_i and K_i are the electronic field shift and mass shift constants, respectively. In a King plot [7], a modified IS $\delta\nu_i^{AA'}/\mu^{AA'}$ for two transitions are plotted against each other for each independent isotope pair, resulting in a straight line as long as Eq. (1) holds.

We have three transitions measured with high precision: $^2S_{1/2} \to {}^2D_{5/2}$ and $^2S_{1/2} \to {}^2D_{3/2}$ in Yb$^+$ (lines a and b, respectively, reported in Ref. [21]), and $^1S_0 \to {}^1D_2$ in Yb (line c, this Letter). In Fig. 2, we present a King plot of line a against line c for our four isotope pairs. The line of best fit is obtained by minimizing χ^2 defined as the sum of the error-weighted distance between each point and the line. The best fit corresponds to $\chi^2 = 70.7$ for two degrees of freedom, implying evidence for nonlinearity at the 8.2σ level.

There are many potential SM sources of NL, as well as NP possibilities. These manifest as additional terms in Eq. (1), so that

$$\delta\nu_i^{AA'} = F_i \delta\langle r^2\rangle^{AA'} + K_i \mu^{AA'} + G_i \lambda^{AA'} + \frac{\alpha_{\rm NP}}{\alpha} D_i \gamma^{AA'}. \quad (2)$$

Here G_i represents additional electronic structure factors associated with SM contributions. In this Letter we consider two higher-order field shift contributions, $G^{(2)}$ and $G^{(4)}$, associated with quadratic field shift ($\lambda = \delta\langle r^2\rangle^2$) and nuclear deformation ($\lambda = \delta\langle r^4\rangle$), respectively. The quantity

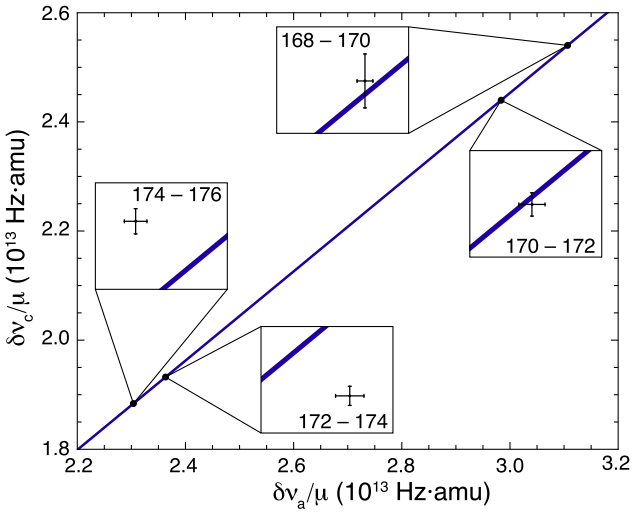

FIG. 2. King-plot comparison of the measured Yb $^1S_0 \to {}^1D_2$ transition (c) and the Yb$^+$ $^2S_{1/2} \to {}^2D_{5/2}$ transition (a) [21]. The inset graphs have width 5×10^7 Hz · amu, and show 1σ error bars that do not include nuclear mass uncertainty since this uncertainty lies parallel to the slope of the King plot F_c/F_a [21,22]. The observed deviation of data points from the best-fit line, i.e., the nonlinearity, has 8.2σ significance.

$\alpha_{\rm NP}/\alpha$ ($\alpha \approx 1/137$ is the fine-structure constant) represents the strength of an additional neutron-electron coupling mediated by the exchange of a light boson of mass m_ϕ, and $\gamma^{AA'} = A' - A$ is the change in neutron number. The electronic factor D_i must be calculated (see the Supplemental Material [29]).

To help distinguish between potential NL sources, and allow us to compare with other transitions in Yb/Yb$^+$, we use the "frequency-normalized" King plot and nonlinearity measures $\zeta_\pm$ introduced in Ref. [21]. In this procedure the isotope-pair-dependent quantities in Eq. (2) are normalized to the reference transition a: $\bar{x}^{AA'} \equiv x^{AA'}/\nu_a^{AA'}$ for $x \in \{\delta\nu_c, \mu, \delta\langle r^2\rangle^2, \delta\langle r^4\rangle, \gamma\}$, leading to the linear relationship

$$\overline{\delta\nu}_c = F_{ca} + K_{ca}\bar{\mu} + G^{(2)}_{ca}\overline{[\delta\langle r^2\rangle^2]} + G^{(4)}_{ca}\overline{\delta\langle r^4\rangle} + \frac{\alpha_{\rm NP}}{\alpha} D_{ca}\bar{\gamma}, \tag{3}$$

where the electronic factors are $F_{ca} = F_c/F_a$ and to lowest order $P_{ca} = P_c - F_{ca}P_a$ for $P \in \{K, G^{(2)}, G^{(4)}, D\}$. The frequency-normalized King plot is constructed by plotting $\overline{\delta\nu}_c = \delta\nu_c/\delta\nu_a$ against $\bar{\mu}$. This plot has a very small slope, so mass uncertainties along the horizontal axis $\bar{\mu}$ have negligible effect.

Vertical deviations of points in the frequency-normalized King plot from the line of best fit d_A are characterized, as in Ref. [21], using the nonlinearity measures

$$\zeta_\pm = d_{168} - d_{170} \pm (d_{172} - d_{174})$$

where the subscript A refers to the isotope pair $(A, A+2)$. In Fig. 3 we plot ζ_- against ζ_+ for different transitions (in all cases we use transition a, Yb$^+$ $6s \to 5d_{5/2}$, as the reference). Also shown are directions in the $\zeta_+ - \zeta_-$ space expected from different NL sources. The current data do not support the majority of NL being due to new physics or a quadratic field shift; however, the possibility of nuclear deformation as the main cause of NL, as discussed in Ref. [26], is still open. To determine the ratio suggested by nuclear deformation, we use experimental values of the nuclear parameters $\langle r^2\rangle$ from Ref. [9] and calculate $\langle r^4\rangle$ using nuclear deformation parameters β [32]. We find that $\overline{\delta\langle r^4\rangle}$ has a ratio of $\arctan(\zeta_-/\zeta_+) = -0.9(0.5)$, consistent with our experimental value of $-0.99(0.13)$. We discuss this further in the Supplemental Material [29].

Generalized King analysis—To place limits on NP we employ the generalized King analysis (GK) [16]. This data-driven method combines the three high-precision transitions in Yb and Yb$^+$ with the calculation of D_i factors (see the Supplemental Material. [29]). In the absence of NL, the modified IS $\vec{\nu}_i \equiv \delta\nu_i^{AA'}/\mu^{AA'}$ for each transition form

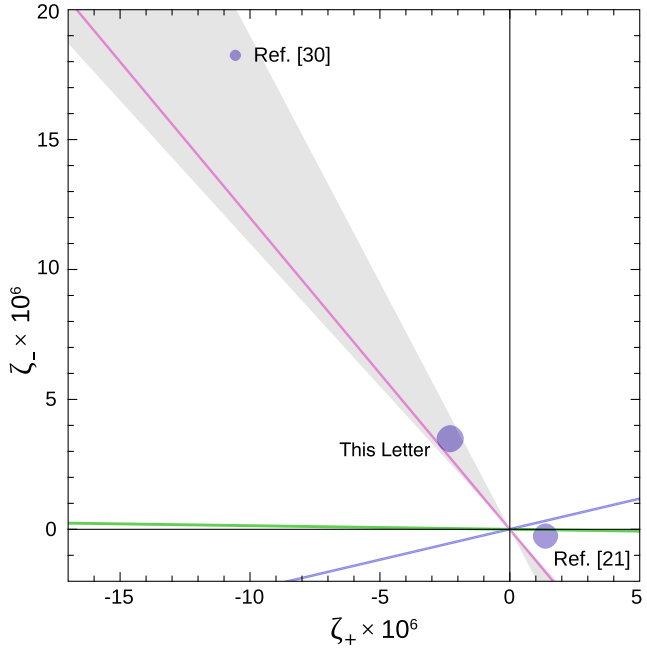

FIG. 3. Nonlinearity measures ζ_- vs ζ_+ (1σ range) for next-neighbor isotope pairs. Straight lines show the directions expected from different NL sources: green line, new physics; blue line, quadratic field shift; pink line, nuclear deformation. The shaded region indicates the 1σ confidence level for the ratio ζ_-/ζ_+ from this Letter.

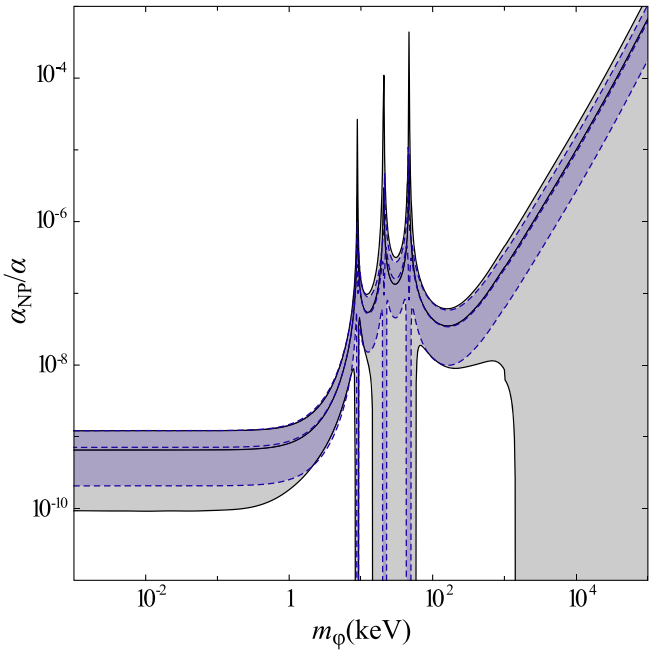

FIG. 4. 95% confidence limits on NP from IS bounds in Yb/Yb$^+$. Blue-shadowed area, range of $\alpha/\alpha_{\rm NP}$ (value and bounds indicated by dashed blue lines) from analysis of two Yb$^+$ lines [21], where there is a 3σ NP signal. Gray-shadowed area, range of $\alpha/\alpha_{\rm NP}$ (value and bounds indicated by black lines) from generalized King-plot analysis of all three lines, which reduces the significance of NP to 2.3σ at small m_ϕ and 1.8σ at large m_ϕ. The reduced significance of NP decreases the lower limit of the allowed NP region. The absence of lower bound indicates that vanishing $\alpha_{\rm NP}$ is consistent with experiment below 2σ.

vectors of dimension four (the number of isotope pairs AA') that all lie in a plane along with the unit vector in isotope space, $\vec{\nu}_\mu = (1,1,1,1)$. Following Ref. [16], we say the dataset is planar provided that the volume $V = \det(\vec{\nu}_a, \vec{\nu}_b, \vec{\nu}_c, \vec{\nu}_\mu)$ is consistent with zero within experimental errors. The NP coupling is then given by

$$\alpha_{\mathrm{NP}} = \frac{V}{V_{\mathrm{th}}(\alpha_{\mathrm{NP}} = 1)}, \tag{4}$$

where V_{th} is the volume formed using the theory ansatz [Eq. (2)] [see Eq. (13) in Ref. [16]]. The benefit of the GK analysis is that it accounts for the dominant SM contribution to NL without relying on knowledge of its size. That is, Eq. (4) does not require a calculation of the G parameters or $\lambda^{AA'}$.

In Fig. 4 we show the NP coupling α_{NP} resulting from this analysis. (To avoid possible confusion with units we present the ratio $\alpha_{\mathrm{NP}}/\alpha$.) The previous results comparing only transitions a and b have a 3σ NL, while the additional use of transition c decreases the NP "detection" to below 2.3σ. This is despite the Yb line showing a large NL when compared in a usual 2D King plot with either of the two Yb^+ transitions. The resonance-like structures are points in m_ϕ where, due to the cancellation of electronic factors D_i from Eq. (2), there is no sensitivity to α_{NP}, and no limits on the allowed range of α_{NP} can be made. At high mass, the significance of NP is 1.8σ, and so the lower bound in Fig. 4 disappears.

Conclusions—Our measurement of the $6s^2\,{}^1S_0 \rightarrow 5d6s\,{}^1D_2$ transition in Yb shows a significant King plot nonlinearity when compared with the Yb^+ transitions of Ref. [21]. We have shown that, unlike in Ref. [21], the majority of this NL cannot be explained by new physics or a quadratic field shift; however, it may still be accounted for by nuclear deformation [26]. Employing the GK analysis to remove the leading SM source of NL reduces the signal for NP to $\sim 2\sigma$.

It is worth pointing out that the Yb transition studied in this Letter has a rather different electronic structure from the transitions in Yb^+ compared in Ref. [21]. This leads to larger differences in the electronic structure factors and hence higher sensitivity to new physics and SM sources that break King linearity. Thus with similar measurement accuracy to Ref. [21], we obtain a more significant NL and a higher sensitivity to distinguishing NL sources as shown in Fig. 3.

Future availability of precision data on additional transitions in either the neutral or ionic Yb may allow for an extension of the GK analysis and evaluation of the remaining NL effect. In the final stages of preparing this Letter, an isotope shift measurement of the Yb $6s^2\,{}^1S_0 \rightarrow 6s6p\,{}^3P_0$ was reported [33]. We have included these data in Fig. 3 and note that the nonlinearity ratio ζ_-/ζ_+ of this transition is consistent with that of the $6s^2\,{}^1S_0 \rightarrow 5d6s\,{}^1D_2$ transition in Yb. This suggests a common origin for the two nonlinearities, but does not assist us in determining the cause. Stronger constraints on new physics can likely be obtained if the effect of nuclear deformation is either accounted for or absent (e.g., in isotopes with spherical nuclei).

We gratefully acknowledge V. Vuletic for insightful communications. This project has received funding from the European Research Council (ERC) under the European Unions Horizon 2020 research and innovation program (Grant Agreement No. 947696) and the Deutsche Forschungsgemeinschaft (DFG)—Project ID No. 423116110. This work was supported by the Cluster of Excellence Precision Physics, Fundamental Interactions, and Structure of Matter (PRISMA+ EXC 2118/1) funded by the DFG within the German Excellence Strategy (Project ID No. 39083149); from the German-Israeli Foundation for scientific research and development (Grant No. 1490); and by the Australian Research Council Grants No. DP190100974 and No. DP200100150, and the JGU Gutenberg Fellowship.

*Corresponding author.
dantypas@uni-mainz.de

[1] B. Roberts, V. Dzuba, and V. Flambaum, Annu. Rev. Nucl. Part. Sci. **65**, 63 (2015).
[2] D. DeMille, J. M. Doyle, and A. O. Sushkov, Science **357**, 990 (2017).
[3] M. S. Safronova, Ann. Phys. (Berlin) **531**, 1970023 (2019).
[4] M. S. Safronova, D. Budker, D. DeMille, Derek F. Jackson Kimball, A. Derevianko, and C. W. Clark, Rev. Mod. Phys. **90**, 025008 (2018).
[5] C. Frugiuele, E. Fuchs, G. Perez, and M. Schlaffer, Phys. Rev. D **96**, 015011 (2017).
[6] J. C. Berengut, D. Budker, C. Delaunay, V. V. Flambaum, C. Frugiuele, E. Fuchs, C. Grojean, R. Harnik, R. Ozeri, G. Perez, and Y. Soreq, Phys. Rev. Lett. **120**, 091801 (2018).
[7] W. H. King, J. Opt. Soc. Am. **53**, 638 (1963).
[8] W. King, *Isotope Shifts in Atomic Spectra* (Springer-Verlag, New York Inc., 1983).
[9] I. Angeli and K. P. Marinova, At. Data Nucl. Data Tables **99**, 69 (2013).
[10] J. A. R. Griffith, G. R. Isaak, R. New, M. P. Ralls, and C. P. van Zyl, J. Phys. B **12**, L1 (1979).
[11] C. Delaunay, R. Ozeri, G. Perez, and Y. Soreq, Phys. Rev. D **96**, 093001 (2017).
[12] V. A. Dzuba, V. V. Flambaum, and Y. V. Stadnik, Phys. Rev. Lett. **119**, 223201 (2017).
[13] D. Antypas, A. Fabricant, J. E. Stalnaker, K. Tsigutkin, V. V. Flambaum, and D. Budker, Nat. Phys. **15**, 120 (2019).
[14] D. Antypas, A. M. Fabricant, J. E. Stalnaker, K. Tsigutkin, V. V. Flambaum, and D. Budker, Phys. Rev. A **100**, 012503 (2019).
[15] V. V. Flambaum, A. J. Geddes, and A. V. Viatkina, Phys. Rev. A **97**, 032510 (2018).

[16] J. C. Berengut, C. Delaunay, A. Geddes, and Y. Soreq, Phys. Rev. Research **2**, 043444 (2020).
[17] S. Origlia, M. S. Pramod, S. Schiller, Y. Singh, K. Bongs, R. Schwarz, A. Al-Masoudi, S. Dörscher, S. Herbers, S. Häfner, U. Sterr, and C. Lisdat, Phys. Rev. A **98**, 053443 (2018).
[18] H. Miyake, N. C. Pisenti, P. K. Elgee, A. Sitaram, and G. K. Campbell, Phys. Rev. Research **1**, 033113 (2019).
[19] T. Manovitz, R. Shaniv, Y. Shapira, R. Ozeri, and N. Akerman, Phys. Rev. Lett. **123**, 203001 (2019).
[20] F. W. Knollmann, A. N. Patel, and S. C. Doret, Phys. Rev. A **100**, 022514 (2019).
[21] I. Counts, J. Hur, D. P. L. Aude Craik, H. Jeon, C. Leung, J. C. Berengut, A. Geddes, A. Kawasaki, W. Jhe, and V. Vuletić, Phys. Rev. Lett. **125**, 123002 (2020).
[22] C. Solaro, S. Meyer, K. Fisher, J. C. Berengut, E. Fuchs, and M. Drewsen, Phys. Rev. Lett. **125**, 123003 (2020).
[23] N.-H. Rehbehn, M. K. Rosner, H. Bekker, J. C. Berengut, P. O. Schmidt, S. A. King, P. Micke, M. F. Gu, R. Müller, A. Surzhykov, and Jose R.Crespo López-Urrutia, Phys. Rev. A **103**, L040801 (2021).
[24] F. Gebert, Y. Wan, F. Wolf, C. N. Angstmann, J. C. Berengut, and P. O. Schmidt, Phys. Rev. Lett. **115**, 053003 (2015).
[25] To observe NL, independent IS data on at least three isotope pairs are needed, so at least four isotopes are required. Isotopes with zero nuclear spin are easier for this analysis, as there is no need to separate the IS from hyperfine structure.
[26] S. O. Allehabi, V. A. Dzuba, V. V. Flambaum, and A. V. Afanasjev, Phys. Rev. A **103**, L030801 (2021).
[27] W. Demtröder, *Laser Spectroscopy 2*, 5th ed. (Springer, New York, 2015).
[28] C. J. Bowers, D. Budker, E. D. Commins, D. DeMille, S. J. Freedman, A.-T. Nguyen, S.-Q. Shang, and M. Zolotorev, Phys. Rev. A **53**, 3103 (1996).
[29] See Supplemental Material at http://link.aps.org/supplemental/10.1103/PhysRevLett.128.073001 for details of experimental methods, data analysis, and calculations of isotope shifts and electronic state-dependent factors.
[30] K. K. Lehmann, J. Chem. Phys. **154**, 104105 (2021).
[31] D. Antypas, A. Fabricant, and D. Budker, Opt. Lett. **43**, 2241 (2018).
[32] S. Raman, C. W. Nestor, and P. Tikkanen, At. Data Nucl. Data Tables **78**, 1 (2001).
[33] K. Ono, Y. Sato, T. Ishiyama, T. Higomoto, T. Takano, Y. Takasu, Y. Yamamoto, M. Tanaka, and Y. Takahashi, arXiv:2110.13544.